Motility of *Escherichia coli* in a quasi-two-dimensional porous medium

Juan Eduardo Sosa-Hernández,[*] Moisés Santillán,[†] and Jesús Santana-Solano[‡]

Centro de Investigación y de Estudios Avanzados del IPN, Unidad Monterrey, Vía del Conocimiento 201,

Parque PIIT, 66600 Apodaca NL, Mexico

Bacterial migration through confined spaces is critical for several phenomena, such as biofilm formation, bacterial transport in soils, and bacterial therapy against cancer. In the present work, *E. coli* (strain K12-MG1655 WT) motility was characterized by recording and analyzing individual bacterium trajectories in a simulated quasi-two-dimensional porous medium. The porous medium was simulated by enclosing, between slide and cover slip, a bacterial-culture sample mixed with uniform 2.98-μm-diameter spherical latex particles. The porosity of the medium was controlled by changing the latex particle concentration. By statistically analyzing several trajectory parameters (instantaneous velocity, turn angle, mean squared displacement, etc.), and contrasting with the results of a random-walk model developed *ad hoc*, we were able to quantify the effects that different obstacle concentrations have upon bacterial motility.

I. INTRODUCTION

Motility is an organism's capability to move in an independent and spontaneous fashion. In general, motility enhances the organism's opportunities to succeed on reproduction and growth, as well as to escape from hazardous environments. *Escherichia coli*'s motility has been thoroughly characterized when it is freely swimming [1–5]. As described in the seminal works of Berg [1,6], *E. coli* swimming consists of alternated runs and tumbles. During runs, swimming is persistent and mostly unidirectional. This motility mode is caused by a bundle of flagella rotating clockwise (forward view) and in phase—due to angular momentum conservation, the bacterium body rotates counterclockwise—and its average duration is about 1 s. Conversely, bacteria constantly reorientate to a random direction during tumbles. Tumbling occurs when at least one flagellum rotates counterclockwise, making the bundle break and the flagella spread. The average duration of tumbles is approximately 0.1 s.

As mentioned before, the bulk motility of *E. coli* has been extensively studied, and this is also true for its motility near solid surfaces [6–10]. However, several questions regarding motility under other conditions remain open. For instance, the effects that confined spaces have on motility have recently become a focus area of research, not only for *E. coli* but also for other living and synthetic microscopic swimmers [11–28]. This interest emerges from the fact that most microorganisms on Earth live in porous environments like soils and biofilms [27,29–33]. Despite these recent advances, it must be emphasized that bacterial motility in micron and submicron constricted spaces has only been studied with ideal geometries [19,28,34–36]. Hence, in order to study bacterial motility in a more realistic environment, we have generated a device that simulates a quasi-two-dimensional porous medium [37], and studied how *E. coli* motility is affected by varying porosity conditions. Our objectives are twofold: (1) experimentally correlate the statistical characteristics of run-and-tumble motility with the density of obstructions and (2) suggest possible explanations for the observed relationships.

II. MATERIALS AND METHODS

A. Cell culture

Escherichia coli cell cultures (wild-type strain MG1655) were prepared from frozen stocks according to the experimental protocol reported in [7]. First, the bacterial culture was saturated by seeding bacteria in lysogeny broth medium (LB, 10 g/L tryptone, 5 g/L yeast extract, and 10 g/L NaCl), and letting them grow for 16 h at 34 °C, shaking at 150 rpm. Next, samples containing 200 μL of the saturated culture, with glycerol at 15% (v/v), were stored at -80 °C. 98 cell culture tubes were prepared from each stock cycle to guarantee consistency between experiments. For each experimental session, a new cell culture was grown from a stock tube by adding 4 mL of fresh LB in 8 mL tubes, containing 200 μL of saturated LB. The resulting cultures were then grown at 34 °C for 3.5 h on a rotary shaker (150 rpm), in order to reach the midexponential phase of bacterial growth. These conditions lead to an OD600 = 0.98. Experimental samples were prepared by washing 1 mL of bacterial culture and resuspending it in fresh motility buffer (10 mM potassium phosphate, 0.1 mM EDTA, 10 mM NaCl; pH = 7.5). Each sample was washed three times by centrifuging the cell culture at 2000 g for 5 min, and dispersing it with fresh motility buffer. Finally, the sample was stored for 15 min, to allow dead and nonmotile bacteria sediment, and medium from the tube top was used to ensure approximately 90% of motile bacteria.

B. Experimental setup

To confine a dilute suspension of bacteria in a quasi-two-dimensional porous medium, we sandwiched a mixture of bacterial culture and 2.98 ± 0.14-μm-diameter polystyrene spheres (Thermo Scientific) between two carefully cleaned glass plates (a slide and a cover slip). To guarantee that the separation between the inner surfaces of the plates coincides with the diameter of the particles, the slide and the cover

* jsosa@cinvestav.mx

† msantillan@cinvestav.mx; http://msantillan.org.mx

‡ jsantana@cinvestav.mx

slip were uniformly pressed one against the other [38]. In our experimental samples, we measured with a confocal microscope [39] the approximate distance between the glass inner surfaces, and obtained in all cases values that lie within the range of the polystyrene-bead diameter reported by the manufacturer. Furthermore, in order to confirm that the polystyrene beads were not deformed due to excess pressure—thus compromising the glass-separation uniformity—we measured the distance between the centers of adjacent beads, whenever they form clusters. Once again, the obtained values lie within the bead-diameter reporter by the manufacturer. From the above considerations, we can ensure that, in our experimental setup, the spherical beads form a monolayer that plays the role of a fixed spacer between the glass plates, and generates a disordered porous matrix in which the beads act as obstacles for bacterial swimming. The obstacle area fraction was controlled by changing the concentration of beads. In our experiments we considered area fraction values ranging from 0.01 to 0.4. In all cases, the bacterial count was kept between 15 and 30 cells within the video field. Evaporation and externally caused fluxes were prevented by sealing the space between glass edges with semipolymerized polydimethylsiloxane (PDMS). The volume of each sample, prepared as we have just described, is about 8 μL. To prevent bacteria from attaching to glass surfaces, slides and coverslips were previously treated with PVP-40 (polyvinylpyrrolidone) in Mili-Q water at 0.005% (w/v) [40]. All experiments were performed at 25 °C. Videos were recorded (at 30 fps, with a resolution of 480 × 720 pixels) by means of a CCD camera mounted on an Olympus BX51 microscope, with a 40× magnification phase contrast objective. With this setup, the frame dimensions are 120 × 160 μm^2. In all cases, the recorded videos were 5 min long.

C. Trajectory analysis

Bacterial trajectories were recovered from the recorded videos via an image-analysis algorithm, originally developed by Crocker and Grier [41], that we implemented on `MatLab`. Basically, this algorithm identifies individual bacteria in every video frame, and then optimizes an adequate objective function to link bacterium positions in consecutive frames. To characterize the obtained trajectories, we computed the instantaneous velocity [$\vec{v}(t)$] and turn angle [$|\theta(t)|$], as well as the mean squared displacement (MSD) [$\langle \Delta \vec{r}(t)^2 \rangle$], by means of the following equations:

$$\vec{r}(t) = x(t)\hat{x} + y(t)\hat{y} + 0\hat{z}, \tag{1}$$

$$\vec{v}(t) = \frac{\vec{r}(t) - \vec{r}(t - \Delta t)}{\Delta t}, \tag{2}$$

$$|\theta(t)| = \cos^{-1}\left(\frac{\vec{v}(t - \Delta t) \cdot \vec{v}(t)}{|\vec{v}(t - \Delta t)||\vec{v}(t)|}\right), \tag{3}$$

$$\langle \Delta \vec{r}(t)^2 \rangle = \langle (\vec{r}(t + n\Delta t) - \vec{r}(t))^2 \rangle, \tag{4}$$

where $\vec{r}(t) = x(t)\hat{x} + y(t)\hat{y} + 0\hat{z}$, Δt is 1/30 s, n is an integer ranging from one to the trajectory length, and $\langle \cdots \rangle$ denotes ensemble average.

Following Masson [42], we measured run and tumble lengths. In our case, runs and tumbles were identified by means

of a Schmitt trigger, in which bacterial speed is the threshold parameter. In summary, when a bacterium speed is above 0.65 times the trajectory mean speed, the bacterium is considered to be in a run. On the other hand, if the bacterium speed is below 0.6 times the trajectory average speed, the bacterium is regarded to be in a tumble [43]. By statistically analyzing all the measured run and tumble times, we found that the corresponding probability density functions (PDFs) are well fitted by exponential distributions of the form

$$\rho(t) = \frac{1}{\tau} e^{-t/\tau}, \tag{5}$$

in which τ is the average residence time.

Finally, for each of the bacterial swimming stages: run and tumble, we performed an analysis of velocity components, using the unitary velocity of the previous step as a reference. We obtained the longitudinal ($\vec{v}_\parallel$) and transverse ($\vec{v}_\perp$) velocity components as follows:

$$\vec{v}_\parallel = \vec{v}(t) \cdot \frac{\vec{v}(t - \Delta t)}{|\vec{v}(t - \Delta t)|}, \tag{6}$$

$$\vec{v}_\perp = \vec{v}(t) \cdot \left(\hat{k} \times \frac{\vec{v}(t - \Delta t)}{|\vec{v}(t - \Delta t)|}\right). \tag{7}$$

After carrying out the corresponding statistical analysis, we found that the experimental PDFs for both the longitudinal and the transverse velocity components, for both motility modes (runs and tumbles), are well fitted by normal distributions:

$$P(x) = \frac{1}{\sigma\sqrt{2\pi}} e^{-(x-\mu)^2/2\sigma^2}, \tag{8}$$

where μ and σ are the distribution mean value and standard deviation, respectively.

III. RESULTS AND DISCUSSION

A. Trajectory analysis at very low obstacle concentration

We recorded bacterial motility videos (following the procedure detailed in the Materials and Methods section) in devices where the obstacle concentration was low enough (obstacle area fraction of 0.01) to keep bacterium-obstacle interactions to a minimum, while ensuring a homogeneous 2.98 μm separation between glass surfaces. We obtained 4202 trajectories with an average length of 1.45 s. Our working assumption was that, at this obstacle concentration, the effects of bacterium-obstacle interactions upon the bacterial-trajectory statistical properties are negligible and so we can employ the obtained results as a control to contrast with further experiments. We measured the instantaneous speed and, as explained in the Materials and Methods section, we used it to classify bacterial swimming as either persistent (runs) or tumbling (tumbles). A typical trajectory is shown in Fig. 1(a), with the run and tumble starting points respectively indicated with green and red marks. The corresponding plot of speed vs time is shown in Fig. 1(b).

After measuring all the run and tumble residence times, we estimated the corresponding probability distribution functions (PDFs), and found that both of them are well fitted by exponential distributions—see Fig. 1(c). The corresponding best fitting parameter values are tabulated in Table I. The observed one-order-of-magnitude difference between the run
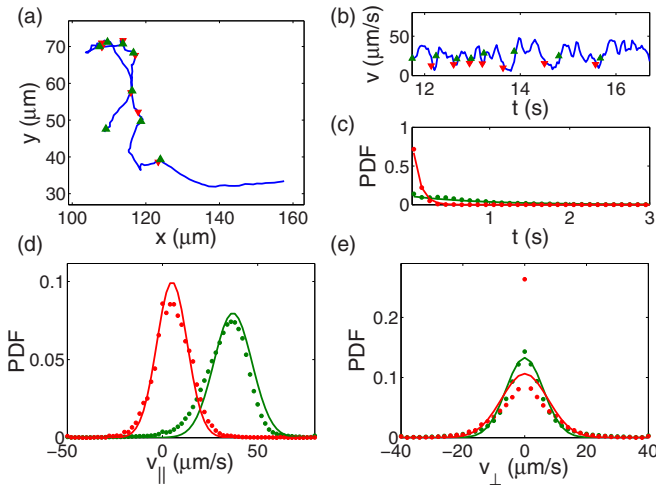
FIG. 1. (a) Typical *E. coli* trajectory at very low obstacle area fraction ($\phi = 0.01$). Run and tumble starting points are respectively indicated with green and red marks. (b) Speed trace for the trajectory in (a). (c) Experimental residence-time PDFs (dots) and best fitting exponential distributions (solid lines) for runs (green) and tumbles (red). (d) Experimental longitudinal velocity PDFs for runs (green dots) and tumbles (red dots), and the corresponding best fitting Gaussian distributions (green and red solid lines). (e) Same as in (d), but for transverse velocity.

and tumble average duration times is consistent with previous reports [6]. The difference between the average run time here observed and previously reported values (corresponding to bacteria swimming in bulk) could be due to interactions with solid surfaces. See for instance the results in [7,9,10,40], in which runs last longer due to hydrodynamic interaction with solid surfaces.

To better characterize bacterial motility under the current experimental conditions, we decomposed the velocity at each trajectory step into components perpendicular and transverse to the previous one. This was done separately for runs and tumbles. Thereafter, we computed the PDFs corresponding to each one of these stages. We found that all the experimental PDFs are well fitted by Gaussian distributions. The experimental and the corresponding best-fitting PDFs for the longitudinal velocity of runs and tumbles are shown in Fig. 1(d). The respective experimental and best fitting

TABLE I. Parameter values for the exponential distributions that best fit the run and tumble residence-time PDFs, as well as for the Gaussian distributions that best fit the longitudinal and transverse velocity PDFs corresponding to both runs and tumbles.

	Residence time			
	Run	Tumble		
τ	1.2 s	0.1 s		
	Velocity components			
	$v_\parallel$ (μm/s)		$v_\perp$ (μm/s)	
	Run	Tumble	Run	Tumble
μ	37.84	5.99	0	0
σ	10.68	8.53	6.09	7.59

distributions for transverse velocity components are shown in Fig. 1(e). The best fitting parameter values for all four PDFs are tabulated in Table I.

We can appreciate in Figs. 1(d) and 1(e) that the longitudinal-velocity mean values corresponding to both runs and tumbles are positive, indicating that bacterial swimming is persistent. Nonetheless, as expected, longitudinal velocities are in general considerably larger during runs than during tumbles. Observe as well that, according to both distributions, the probability of having negative longitudinal velocities is non-negligible. These negative values make possible for bacteria to reverse or turn 180°, and this feature in turn allows bacteria to escape bead traps by reversing their swim as described in [2,4,5,44,45]. Finally, notice that the transverse velocity distributions are symmetrical and they have zero mean values.

B. Mathematical modeling

The former subsection results suggest that, when bacterium-obstacle interactions are negligible, bacterial swimming can be described as a random walk with the following characteristics:

(i) Bacteria flip between two different motility modes: runs and tumbles. The random walk corresponding to runs is more persistent in the forward direction than that corresponding to tumbles.

(ii) Transitioning between runs and tumbles is dictated by a random process with mean residence times as tabulated in Table I.

(iii) In both motility modes, each bacterium step can be regarded as the sum of components longitudinal and transverse to the previous step. These components obey independent Gaussian distributions whose parameters are tabulated in Table I for both, runs and tumbles.

Based on this description, we implemented the following algorithm to simulate bacterium trajectories at very low obstacle concentrations.

(1) Set the time step $\Delta t = 1/30$ s.

(2) Set the initial simulation time to $t = 0$, and randomly choose the x and y coordinates of the initial trajectory point from uniform distributions in the ranges $[0, 160]$ μm and $[0, 120]$ μm, respectively.

(3) Randomly select the initial motility mode: persistent or tumbling, considering a probability of 0.5 for each one.

(4) Randomly compute, from the PDF in Eq. (5), the time T the simulated bacterium will remain in the current motility mode. To do this, consider the parameter values of the corresponding motility mode.

(5) Calculate the number of steps to be given in the current mode as the integer part of $N = T/\Delta t$.

(6) For every step, randomly calculate the velocity longitudinal and transverse component by means of the PDF in Eq. (8), with the corresponding parameter values. Then, multiply times Δt to get the corresponding displacement, and update the bacterium position accordingly.

(7) Update the simulation time, $t := t + N\Delta t$.

(8) Switch motility to the other mode.

(9) Iterate from step (4).

To test whether our description of bacterial swimming is accurate, we employed the above algorithm to simulate
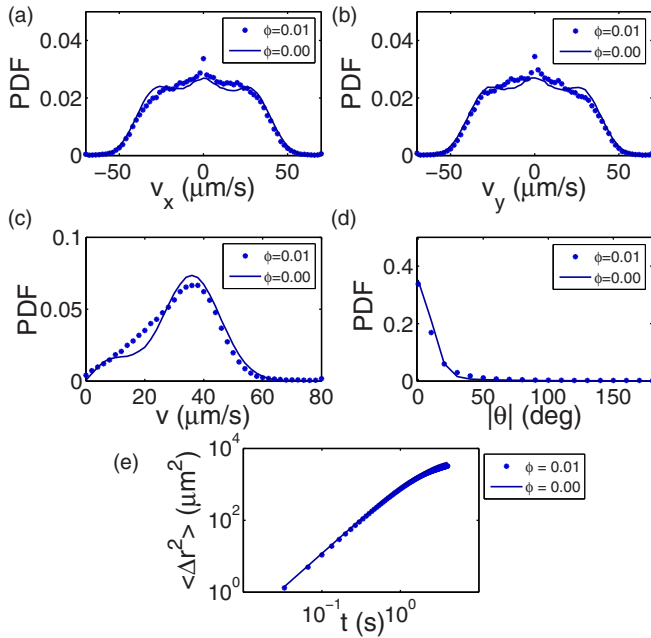
FIG. 2. Statistical characteristics of trajectories recorded at very low obstacle concentrations ($\phi = 0.01$)—symbols—and of simulated trajectories under the same conditions—lines. (a) Probability density function (PDF) for the velocity component along the x axis. (b) PDF for the velocity component along the y axis. (c) Speed probability density function. (d) PDF for the turn angle between consecutive steps. (e) Mean squared displacement (MSD) from all bacterial trajectories.
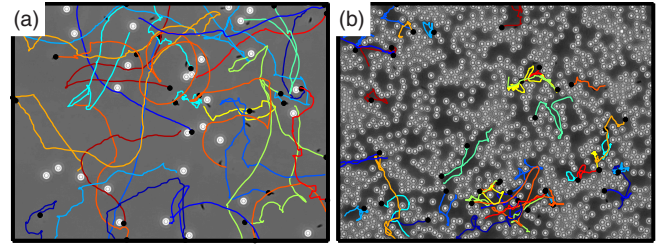

FIG. 3. Experimental bacterial trajectories under low and high obstacle-area-fraction conditions: (a) $\phi = 0.01$ and (b) $\phi = 0.39$. Obstacles are represented as white circles.

more than 9000 trajectories with an average length of 3.53 s in a 120×160 μm surface, considering periodic boundary conditions. Thereafter, we statistically analyzed the simulated trajectories and compared the results with those obtained from the experiments. We measured bacterium velocity along all trajectory steps, and decomposed it into components parallel to arbitrary horizontal and vertical axes. Then, we computed the corresponding probably density functions (PDFs), plotted the results in Figs. 2(a) and 2(b), and verified the agreement between the results from the experimental and the simulated trajectories. It is also worth emphasizing that the PDFs for the horizontal and vertical velocity components are almost identical, and that both of them are symmetrical and centered in the origin. This is important because it evidences the absence of external fluxes and chemotaxis in our experimental setup.

We also computed the speed in all trajectory steps, as well as the turn angle between consecutive steps. The corresponding PDFs are shown in Figs. 2(c) and 2(d) for the simulated and the experimental trajectories. Once again, notice the good agreement between simulated and experimental results. One interesting feature that can be observed in the speed PDF curve corresponding to simulations is that it is bimodal. The large speed mode corresponds to runs, while the low speed mode corresponds to tumbles. This feature is not apparent in the corresponding experimental PDF, presumably due to lack of statistics. Finally, we computed the mean squared displacement (MSD) from all bacterial trajectories, and show the results in Fig. 2(e). Observe how the MSD curves

obtained from the simulated and the experimental trajectories overlap almost perfectly. In these curves we can observe that the transition from ballistic to diffusive motion takes place between about 0.2 and 1.0 s.

C. Effect of increasing obstacle concentration

At this point, we can assert from the results in the previous section that we have an accurate description of *E. coli* motility, when it is constrained to move in a quasi-two-dimensional environment. In what follows, we shall use this description as a point of comparison to understand the effects that increased obstacle concentrations have on this bacterium motility. To achieve this goal, we recorded motility videos while gradually increasing obstacle concentration, up to an obstacle area fraction of about 0.4. In total, we obtained 88 videos, and at least two of them correspond to each one of the considered area fractions. As described in the Materials and Methods section, we recovered all the possible bacterial trajectories from the recorded videos. On average, we were able to obtain 2690 trajectories from every video, the average trajectory length being 46 steps (about 1.5 s).

In Figs. 3(a) and 3(b) we show representative samples of the trajectories we got from typical videos recorded at low (a) and high (b) obstacle area fractions. We can appreciate that bacterial trajectories display noticeable changes as the obstacle concentration increases. For instance, at low obstacle concentrations, bacterium swimming is more persistent than it is at higher obstacle concentrations. On the other hand, obstacle arrangement at high concentrations makes it possible to find several configurations such as: corridors, chambers, and inaccessible areas, all of which seem to affect bacterial motility.

After carefully inspecting the recorded motility videos, obtained at different obstacle concentrations, we noticed that the presence of obstacles affects bacteria in different ways as follows.

(i) Given that in our experimental setup, the confinement due to the glass walls is of the same order as bacterium size (or even smaller, if the flagellar bundle is also considered), bacteria do not possess long-range hydrodynamic interactions with either each other or with obstacles, but they sense an overall increase in friction, and this effect is enhanced as the obstacle area fraction increases.

(ii) Besides the previously described global effect, we also noticed that bacteria interact individually with obstacles. These interactions, which can be either steric or short-range

hydrodynamic interactions, have the following effects: (a) obstacles have an effective cross section which is larger than their physical size, (b) bacterium-obstacle interactions increase the probability of run-to-tumble shifts, and (c) bacteria swim around obstacles after a collision.

To account for these observations, we modified the algorithm we employed to generate simulated trajectories as follows (the reported parameter values were obtained by trial and error, so that the simulation results resemble the experimental ones).

(i) The above discussed increase in friction was taken into consideration as follows. If the simulated bacterium is in the persistent motility mode (i.e., in a run), instead of randomly computing the longitudinal velocity component from a Gaussian distribution with the mean value reported in Table I, we took $\mu = \mu_0(1 - m\phi)$, with $\mu_0 = 37.84$ μm/s, and $m = 0.76$.

(ii) Solid disk obstacles with a radius of 2 μm ($\approx$33% larger than the radius of the polystyrene beads) were placed in the same positions the beads have in the recorded videos.

(iii) If, as the result of a trajectory step, the simulated bacterium would penetrate or swim across an obstacle, we allow the bacterium to reach the obstacle edge, and then we make it swim for a given distance $d \leqslant l$ (with l the length of the original step minus the distance traveled up to the obstacle edge) along the obstacle edge. We call this an "arch"-type collision.

(iv) When a bacterium that is in a run collides with an obstacle, its motility mode changes to tumbling with a probability of 0.4, as a result of the collision.

After modifying the algorithm to account for bacterium-obstacle interactions, we simulated several trajectories (9535, 4619, 2879, 1549, and 1094, each one respectively being 105.87, 158.78, 197.65, 247.62, and 277.64 steps long, with a sampling frequency of 30 fps), for every one of the following obstacle area fractions: $\phi = 0.01, 0.1, 0.2, 0.29, 0.39$. In what follows, we compare the results from experimental and simulated trajectories.

First, we measured the horizontal (v_x) and vertical (v_y) velocity components at every step and calculated the corresponding probability density functions. The results are shown in Fig. 4. There, we can appreciate that all PDFs are symmetrical and that the v_x and v_y probability distributions are very much alike. These results allow us to disregard both

FIG. 5. (a) Speed probability density functions (PDFs) computed from experimental (symbols) and simulated (solid lines) trajectories at various obstacle area fractions (ϕ): blue, $\phi = 0.01$; cyan, $\phi = 0.1$; green, $\phi = 0.2$; light brown, $\phi = 0.29$; red, $\phi = 0.39$. (b) Turn-angle PDFs computed from experimental (symbols) and simulated (solid lines) trajectories at various obstacle area fractions. The color code is the same as in (a).

external fluxes and chemotaxis in our experimental setup. Moreover, the PDFs narrow as the obstacle area fraction (ϕ) increases. This is in agreement with our previous appreciation that the average bacterium speed decreases as ϕ increases. The simulated trajectory results agree well with those from experimental ones.

To further characterize how bacterial motility is affected by the presence of different obstacle concentrations, we measured the instantaneous speed from all experimental and simulated trajectories, and computed the corresponding probability density functions (one for each obstacle area fraction). The results are shown in Fig. 5(a). Note that, once more, there is a good agreement between the simulated and the experimental results. Although it is not so clear in the experimental curves, we can see in the speed PDFs computed from simulated curves that either they are bimodal or they have a shoulder. In either case, this behavior can be understood as the weighted addition of two monomodal PDFs corresponding to runs and tumbles. Taking this into consideration, we can appreciate that the weight of the mode corresponding to tumbles increases together with the obstacle area fraction. This is concomitant with the model assumption that run-to-tumble transitions increase as a consequence of bacterium-obstacle interactions. Moreover, the mode (most probable speed value) corresponding to runs decreases as the obstacle concentration increases. As far as we understand, this is due to the effective friction increase that bacteria sense as a result of the dense confinement caused by obstacles. Finally, observe that all PDFs are heavy tailed and, in consequence, there is a non-negligible probability that bacteria move with speeds as large as 50 μm/s—even at the higher obstacle concentrations. A careful inspection of the recorded videos revealed that this behavior is associated to the existence of long corridors along whose centers bacteria can swim in a mostly rectilinear fashion.

The turn angle between consecutive steps is another helpful parameter to characterize complex trajectories. We measured this parameter from all the experimental and simulated trajectories, computed the corresponding PDFs (one for every considered obstacle area fraction), and plotted the results in Fig. 5(b). Observe that the turn-angle PDFs become wider and heavier tailed as the obstacle concentration increases. This means that, as expected, turn angles increase due to
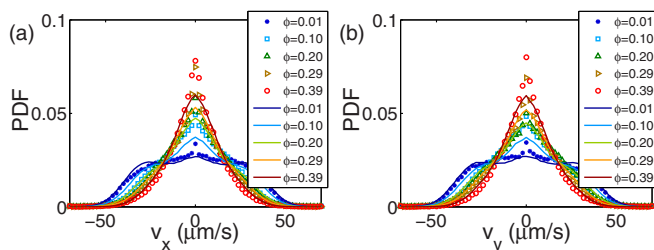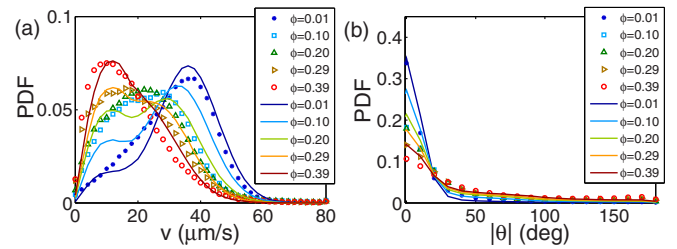

FIG. 4. Probability density functions for the bacterium horizontal (v_x) and vertical (v_y) velocity components, calculated from experimental (symbols) and simulated (solid lines) trajectories, at different obstacle area fractions (ϕ): blue, $\phi = 0.01$; cyan, $\phi = 0.1$; green, $\phi = 0.2$; light brown, $\phi = 0.29$; red, $\phi = 0.39$.
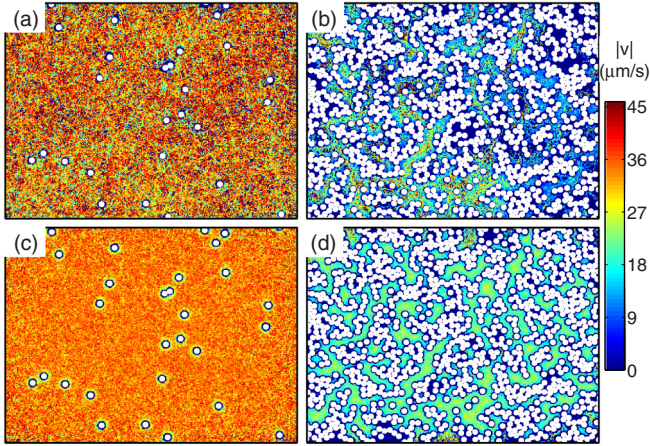
FIG. 6. Mean speed (averaged over time and over all trajectories in every squared micron) maps computed from experimental—(a) and (b)—and simulated—(c) and (d)—trajectories at different obstacle concentrations (same experiments as those in Fig. 1). The color code is given in the adjacent bar. Spherical beads are represented as white circles.
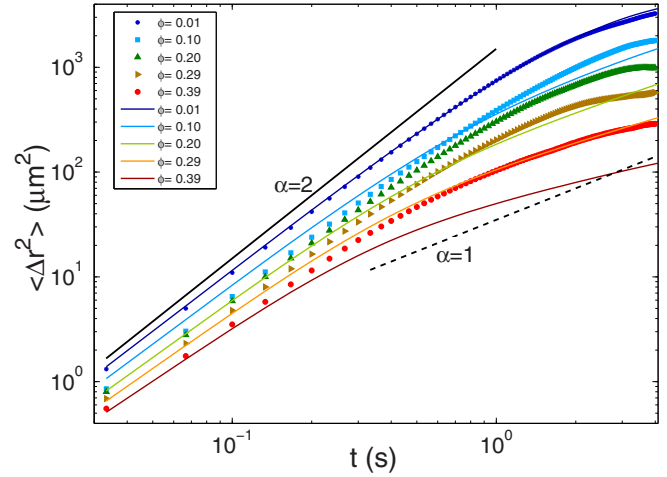

FIG. 7. Plots of mean squared displacement (MSD) vs time, computed from experimental (symbols) and simulated (solid lines) trajectories, at different obstacle area fractions (ϕ).

bacterium-obstacle concentrations. On the other hand, we can observe by contrasting the experimental and the simulated results that the PDFs computed from the simulated trajectories render larger values at low turn angles, and that this difference becomes more notorious at larger obstacle concentrations. We believe that this discrepancy is due to the model assumption that the obstacles behave as solid disks when they interact with bacteria, while in reality this is not true. By inspecting the videos, we noticed that, in fact, obstacles interact with bacteria with a larger effective cross section than their physical size. However, they do not necessarily behave as hard disks. In particular, we observed that, in some instances, a swimming bacterium could sense an obstacle at a short distance (1–2 μm) and smoothly correct its trajectory to avoid a collision. Since our model does not account for this behavior, it most likely underestimates interactions that deflect bacterium trajectories at longer distances than the effective obstacle radius.

To continue the comparison between simulated and experimental results, we measured the average bacterial speed (averaged over time and over all available trajectories) in every squared micron of the recorded field, and plotted the results in Fig. 6 for the experimental and the simulated trajectories. Notice the good qualitative agreement between the experimental and the simulated results. The observed differences at low obstacle concentration [Figs. 6(a) and 6(c)] can be explained by lack of statistics regarding experimental trajectories. In both the experimental and the simulated trajectories, the average bacterial speed decreases in the neighborhood of obstacles, and this phenomenon is more prominent as the obstacle concentration increases. According to the model results, this behavior is due to the increased probability of run-to-tumble transitions due to bacterium-obstacle interactions. Moreover, the simulated trajectories are also able to reproduce that, when larger obstacle concentrations lead to corridors, chambers, and inaccessible areas, bacterial speed in corridors and chambers is about 25 μm/s and 15 μm/s, respectively. That is, bacterial

motility at high obstacle concentrations is severely affected but not completely stopped, and bacteria are still able to escape from traps and visit most of the available space. These results also follow from the model assumption that bacteria are differently affected in the vicinity of obstacles and far away from them. As previously explained, all bacteria sense an increased friction due to physical constraints imposed by obstacles, but their run-and-tumble behavior is also affected by collisions.

Finally, we computed the mean squared displacement (MSD) from both the experimental and the simulated trajectories, and present the results in Fig. 7. There, we can appreciate that, in both cases, the MSD slope is negatively correlated to the area fraction occupied by obstacles. Moreover, at short times, all MSD's denote superdiffusive motion, as expected for autopropulsive colloidal particles. Also expected is the fact that the duration of superdiffusive motion decreases as obstacle concentration increases. This happens because the distance bacteria swim without interacting with obstacles decreases with obstacle concentration. Furthermore, we can notice that at short times ($\lesssim 0.2$ s) there is a good agreement between the MSD curves from the experimental and the simulated trajectories. However, superdiffusive motion lasts shorter in the simulated trajectories than in the experimental ones, and this explains the discrepancy observed between MSDs obtained from simulated and experimental trajectories at longer times. As far as we understand, this discrepancy can also be explained by the model supposition that obstacles behave as hard disks when they interact with bacteria. As we have explained, because of this assumption, the model underestimates short range interactions that make bacteria neither shift from runs to tumbles, nor make tight turns. However, in order to reproduce the speed related statistics, we had to compensate with collisions that potentially have such effects, and so they shorten the average duration of superdiffusive motion. Another possible explanation is that, in the videos, some trapped bacteria can swim backwards to escape, and we do not consider this possibility in the model.

IV. EFFECTS OF MODIFYING THE MODEL FEATURES

The previous section results suggest that (a) long-range hydrodynamic interactions are unimportant for cells in porous media, (b) obstacles increase the effective friction encountered by cells as they swim, and (c) the statistics of cell trajectories are dominated by the details of short range bacterium-obstacle interactions. The first two points are not unexpected because they agree with previously published experimental and theoretical reports. On the other hand, the third point constitutes the present work's main contribution. Regarding this, according to our simulation results, bacterium-obstacle interactions are as follows.

(i) All collisions are of the "arch" type.

(ii) Obstacles have a larger effective size in simulations to account for any sensing of their presence by cells.

(iii) Running cells can switch with a certain probability to tumbling after reaching an obstacle.

Although the present model allowed us to reproduce the statistical characteristics of experimental trajectories, it is necessary to explore the model behavior when bacterium-obstacle interactions are modified because the proposed interactions correspond to new hypotheses regarding cell behavior in confined geometries. Furthermore, although *E. coli* is well studied, it is by no means a model organism and so it is possible that a wider exploration of the model predictions could be important for other run-and-tumble micro-organisms. In accordance with the former discussion, we carried out several simulations in which we changed either the probability of run-to-tumble transitions after a collision, the obstacle effective size, and the type of collision (tangential deflection instead of arch). The results obtained after analyzing the statistical characteristic of the simulated trajectories are summarized in Figs. 8–10.

In Fig. 8 we can appreciate the effects of changing the probability that a running bacterium shifts to tumbling after a
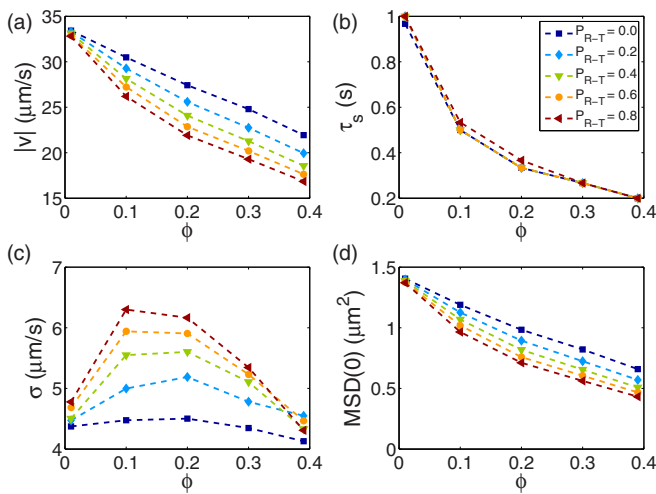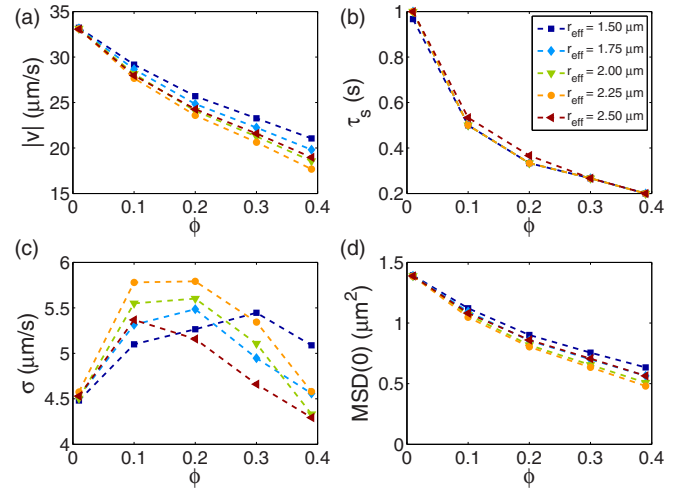

FIG. 9. Plots of mean bacterial speed (a), duration of the MSD superdiffusive phase (b), standard deviation across the mean speed maps (c), and extrapolation of the MSD value at $t = 0$ (d) vs the obstacle area fraction (ϕ) for different values of the obstacle effective radius (r_{eff}) and for a run-to-tumble transition probability after a bacterium-obstacle collision $P_{R-T} = 0.4$.

collision, P_{R-T}. Note that bacterial mean speed decreases as P_{R-T} increases. Although we don't show the corresponding speed probability distribution functions, we could corroborate that, as one would expect, the observed bacterial-mean-speed decrease is due to a relative increase of the mode corresponding to tumblings. We also estimated the mean squared displacement value at time $t = 0$, MSD(0). Observe that increasing P_{R-T} has similar effects on the bacterial mean speed and MSD(0). This can be explained taking into account that at very short times the MSD corresponds to ballistic motion, MSD $\approx (\bar{v}t)^2$ with $\bar{v}$ the bacterium mean

FIG. 8. Plots of mean bacterial speed (a), duration of the MSD superdiffusive phase (b), standard deviation across the mean speed maps (c), and extrapolation of the MSD value at $t = 0$ (d) vs the obstacle area fraction (ϕ) for different values of the run-to-tumble transition probability after a bacterium-obstacle collision (P_{R-T}) and for an effective obstacle radius $r_{\text{eff}} = 2 \mu$m.
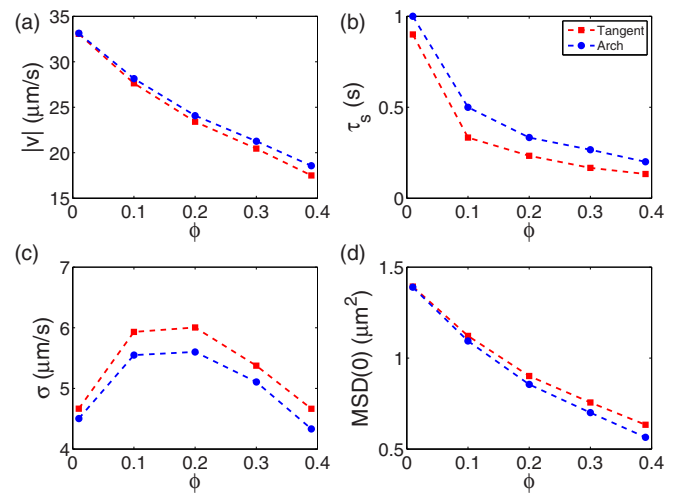

FIG. 10. Plots of mean bacterial speed (a), duration of the MSD superdiffusive phase (b), standard deviation across the mean speed maps (c), and extrapolation of the MSD value at $t = 0$ (d) vs the obstacle area fraction (ϕ) for two different types of bacterium-obstacle collisions (for $P_{R-T} = 0.4$ and $r_{\text{eff}} = 2 \mu$m): "arch" and tangential deflections.

speed, and so MSD(0) $\approx 2 \ln \bar{v} + 2 \ln t$. Furthermore, we can see in Fig. 8 that the probability P_{R-T} has no noticeable effect on the duration of the superdiffusive phase because it decreases in a similar way as the obstacle area fraction (ϕ) increases, regardless of the P_{R-T} value. Finally, in order to quantify the spatial heterogeneity of the average bacterial speed, we measured the standard deviation (σ) of the average bacterial speed values in every squared micron of the recorded field (see Fig. 6). We can observe in Fig. 8 that σ is a concave function ϕ with a single maximum. This happens because the run-to-tumble shifts caused by collisions cause the bacterial average speed to decrease in the neighborhood of obstacles. Thus, when obstacle concentration is very low, the average bacterial speed is quite homogeneous because the area adjacent to obstacles is negligible. Moreover, when obstacle concentrations are very high, the average bacterial speed also tends to be homogeneous because most of the free area is adjacent to obstacles. In agreement with the above discussion, the maximum σ value (which is reached at about $\phi \approx 0.2$) increases as P_{R-T} increases.

The influence that changing the obstacle effective radius has upon bacterial trajectories is summarized in Fig. 9. Note that the bacterial mean speed is not affected by the value of the obstacle mean radius at very low obstacle concentrations. However, as ϕ increases, larger obstacle effective radii imply lower bacterial mean speed values. To the best of our understanding, this happens because the probability of bacterium-obstacle collisions increases with larger obstacle effective radii. Regarding the duration of the superdiffusive phase, we can observe in Fig. 9 that it is not affected by the obstacle effective radius. Finally, it is possible to observe in Fig. 9 that although the maximum σ value does not change much as the effective obstacle radius increases, its position moves to the left on the ϕ axis. In agreement with the discussion in the previous paragraph, we argue that this occurs because when the effective obstacle size increases, fewer of them are required to decrease the free area a given proportion.

To conclude our analysis, we present in Fig. 10 a comparison of the effects of arch and tangential-deflection collisions. As we can appreciate, changing the collision type has a minimum effect on the bacterial mean speed; changing from arch to tangential-deflection collisions decreases the duration of superdiffusive motion (we believe this happens because with tangential deflection collisions a bacterium reaches other obstacles more rapidly than with arch collisions); and the maximum σ value is larger for tangential deflections than it is for arch collisions. Thus, at long times, the mean squared

displacement obtained with tangential deflection collisions is much smaller than the corresponding experimental result.

After modifying various features of the model, we could see that in most cases the consequences were relatively easy to explain. However, given the model's phenomenological nature, more work is necessary to understand the mechanisms that could make the model features change. This would be of particular importance to employ the present modeling strategy to study the motility in porous media of other microbial swimmers.

V. CONCLUSIONS

We have designed a device to simulate a quasi-two-dimensional porous medium with 2.98-μm-diameter latex beads, and have studied how the medium porosity (which we control by means of bead concentration) affects *E. coli* motility. We found that the constraints imposed by the device itself, as well as by the latex beads, preclude long-range hydrodynamic interactions, but cause bacteria to sense an increased friction—which increases more-or-less linearly with the obstacle concentration. Besides this global (mean-field-like) effect, we could also identify other phenomena arising from direct bacterium-bead interactions, specifically as follows.

(i) The latex beads interact with bacteria with an effective cross section that is larger than its physical size. This can be explained by means of very short range hydrodynamic interactions, and/or by steric interactions with bacterium flagella.

(ii) Bacterium-obstacle interactions increase the probability of run-to-tumble shifts.

We corroborated these conclusions by developing a random-walk model that incorporates the above described interactions and is able to reasonably reproduce the statistical characteristics of the trajectories experimentally obtained with different latex-bead concentrations. Finally, the behavior of the model when its features accounting for bacterium obstacle interactions are modified was also investigated.

ACKNOWLEDGMENTS

[1] H. C. Berg and D. A. Brown, Nature (London) **239**, 500 (1972).

[2] H. C. Berg and L. Turner, Proc. Natl. Acad. Sci. USA **92**, 477 (1995).

[3] M. Wu, J. W. Roberts, S. Kim, D. L. Koch, and M. P. DeLisa, Appl. Environ. Microbiol. **72**, 4987 (2006).

[4] L. Turner, W. S. Ryu, and H. C. Berg, J. Bacteriol. **182**, 2793 (2000).

[5] L. Turner, R. Zhang, N. C. Darnton, and H. C. Berg, J. Bacteriol. **192**, 3259 (2010).

[6] H. C. Berg, in *E. coli in Motion*, edited by H. C. Berg, Biological and Medical Physics, Biomedical Engineering (Springer, New York, 2004).

[7] E. Lauga, W. R. DiLuzio, G. M. Whitesides, and H. A. Stone, Biophys. J. **90**, 400 (2006).

[8] K. Drescher, R. E. Goldstein, N. Michel, M. Polin, and I. Tuval, Phys. Rev. Lett. **105**, 168101 (2010).

[9] K. Drescher, J. Dunkel, L. H. Cisneros, S. Ganguly, and R. E. Goldstein, Proc. Natl. Acad. Sci. USA **108**, 10940 (2011).

[10] D. Giacché, T. Ishikawa, and T. Yamaguchi, Phys. Rev. E **82**, 056309 (2010).

[11] A. T. Brown, I. D. Vladescu, A. Dawson, T. Vissers, J. Schwarz-Linek, J. S. Lintuvuori, and W. C. K. Poon, Soft Matter **12**, 131 (2016).

[12] P. K. Ghosh, J. Chem. Phys. **141**, 061102 (2014).

[13] S. E. Spagnolie, G. R. Moreno-Flores, D. Bartolo, and E. Lauga, Soft Matter **11**, 3396 (2015).

[14] D. Takagi, J. Palacci, A. B. Braunschweig, M. J. Shelley, and J. Zhang, Soft Matter **10**, 1784 (2014).

[15] G. Volpe, I. Buttinoni, D. Vogt, H.-J. Kummerer, and C. Bechinger, Soft Matter **7**, 8810 (2011).

[16] X. Zheng, B. ten Hagen, A. Kaiser, M. Wu, H. Cui, Z. Silber-Li, and H. Löwen, Phys. Rev. E **88**, 032304 (2013).

[17] T. Brotto, J.-B. Caussin, E. Lauga, and D. Bartolo, Phys. Rev. Lett. **110**, 038101 (2013).

[18] J. P. Hernandez-Ortiz, C. G. Stoltz, and M. D. Graham, Phys. Rev. Lett. **95**, 204501 (2005).

[19] M. Jabbarzadeh, Y. K. Hyon, and H. C. Fu, Phys. Rev. E **90**, 043021 (2014).

[20] E. Lushi, H. Wioland, and R. E. Goldstein, Proc. Natl. Acad. Sci. USA **111**, 9733 (2014).

[21] A. Najafi, S. S. H. Raad, and R. Yousefi, Phys. Rev. E **88**, 045001 (2013).

[22] M. Sandoval and L. Dagdug, Phys. Rev. E **90**, 062711 (2014).

[23] G. Lambert, D. Liao, and R. H. Austin, Phys. Rev. Lett. **104**, 168102 (2010).

[24] Z. W. Liu and K. D. Papadopoulos, Appl. Environ. Microbiol. **61**, 3567 (1995).

[25] J. Rutllant, M. López-Béjar, and F. López-Gatius, Reprod. Dom. Anim. **40**, 79 (2005).

[26] M. B. Wan, C. J. Olson Reichhardt, Z. Nussinov, and C. Reichhardt, Phys. Rev. Lett. **101**, 018102 (2008).

[27] K. Kusy and R. M. Ford, Environ. Sci. Technol. **41**, 6403 (2007).

[28] L. Ping, V. Wasnik, and E. Emberly, FEMS Microbiol. Ecol. **91**, 1 (2015).

[29] M. Binz, A. P. Lee, C. Edwards, and D. V. Nicolau, Microelectron. Eng. **87**, 810 (2010).

[30] C. Jimenez-Sanchez, L. Y. Wick, and J.-J. Ortega-Calvo, Environ. Sci. Technol. **46**, 6790 (2012).

[31] M. S. Olson, R. M. Ford, J. A. Smith, and E. J. Fernandez, Environ. Sci. Technol. **39**, 149 (2005).

[32] M. S. Olson, R. M. Ford, J. A. Smith, and E. J. Fernandez, Bioremed. J. **10**, 13 (2006).

[33] J. W. Barton and R. M. Ford, Appl. Environ. Microbiol. **61**, 3329 (1995).

[34] J. Mannik, R. Driessen, P. Galajda, J. E. Keymer, and C. Dekker, Proc. Natl. Acad. Sci. USA **106**, 14861 (2009).

[35] I. Berdakin, Y. Jeyaram, V. V. Moshchalkov, L. Venken, S. Dierckx, S. J. Vanderleyden, A. V. Silhanek, C. A. Condat, and V. I. Marconi, Phys. Rev. E **87**, 052702 (2013).

[36] M. Raatz, M. Hintsche, M. Bahrs, M. Theves, and C. Beta, Eur. Phys. J. Spec. Top. **224**, 1185 (2015).

[37] Y. Davit, H. Byrne, J. Osborne, J. Pitt-Francis, D. Gavaghan, and M. Quintard, Phys. Rev. E **87**, 012718 (2013).

[38] G. Cruz de León and J. L. Arauz-Lara, Phys. Rev. E **59**, 4203 (1999).

[39] Leica TCS SP5 Inverted Confocal Microscope, operated in the transmitted light mode. $63\times$ oil-immersion objective with numerical aperture of 0.60. Images were taken with a spatial resolution of 512×512 pixels.

[40] A. P. Berke, L. Turner, H. C. Berg, and E. Lauga, Phys. Rev. Lett. **101**, 038102 (2008).

[41] J. Crocker, J. Crocker, and D. Grier, J. Colloid Interface Sci. **179**, 298 (1996).

[42] J.-B. Masson, G. Voisinne, J. Wong-Ng, A. Celani, and M. Vergassola, Proc. Natl. Acad. Sci. USA **109**, 1802 (2012).

[43] We chose these specific parameter values because they rendered a good comparison between the obtained classification of runs and tumbles and our own visual analysis of the recorded videos. We also tried changing the values of these parameters and the resulting statistical characteristics of the analyzed trajectories were quite robust to variations as large as 20%.

[44] L. Cisneros, C. Dombrowski, R. E. Goldstein, and J. O. Kessler, Phys. Rev. E **73**, 030901 (2006).

[45] S. Bianchi, F. Saglimbeni, A. Lepore, and R. Di Leonardo, Phys. Rev. E **91**, 062705 (2015).